Stanford Exploration Project, Report 79, November 16, 1997, pages 1–153

Controlled illumination by wavefront synthesis

Jun Ji[1]

keywords: *imaging, depth migration, velocity, acquisition, prestack, synthetic data, diffraction*

ABSTRACT

Controlled illumination by wavefront synthesis is a depth migration which is tuned by adopting the wavefront synthesis technique. This imaging method provides several advantages over conventional prestack depth migration. One is computational efficiency, the second is the quality of the images, and the third is that it provides more information about reflectors, such as angle dependent reflection coefficients.

INTRODUCTION

It has long been recognized that the one of the most accurate ways to image areas that are geologically complex is prestack depth migration. Many prestack depth migration algorithms have been developed and applied to common shot gathers or common receiver gathers. This approach, however, is not efficient in computation, especially in 3D. Full prestack depth migration still requires too much time for routine processing even in 2D.

An alternative process to full prestack depth migration is migration of a stack that is based on wavefront reconstruction. Huygens' principle of superposition permits the synthesis of arbitrarily shaped downward propagating wavefronts from many spherical wavefronts. Imaging or processing based on wavefront synthesis has been considered in seismic exploration. Taner (1976) proposed to synthesize plane wave sources at the surface by stacking traces in a common receiver gather. Later, Schultz and Claerbout (1978) showed a way to observe angle-dependent reflection coefficients by synthesizing a slanted plane wave source. Recently, Rietveld et al. (1992) and Rietveld and Berkhout (1992) presented the "optimum seismic illumination technique" by synthesizing a plane wave at a specified depth.

This paper reviews the profile imaging technique as a conventional prestack depth migration with its limits and problems. Optimum seismic illumination (Rietveld, et al, 1992) is reviewed in terms of how it overcomes the hurdles of conventional depth

[1]**email:** not available

migration and tested with the Marmousi data. Some discussions are given about the problems of the optimum illumination and possible improvements to pursue in the future.

OPTIMUM IMAGE

The main purpose of migration is to obtain an accurate image of the subsurface. This image is used to interpret the structure and identify the composition of the subsurface. We usually consider the image obtained by migration as a map of the averaged reflection coefficients. For use in a structural interpretation, some large values along the reflector to increase the contrast of the reflector image from background noise would be sufficient. For the identification of the subsurface rock properties, however, the image must be clarified in terms of the relation to the true reflection coefficient.

The reflection coefficient is a function of the angle of incidence at a reflector. In order to describe a reflector completely, therefore, the image should be multi-valued, with each image determined by the angle-dependent reflection coefficient. Or it can be represented by a single value which characterizes the reflector, such as the maximum reflection coefficient, the reflection coefficient of the normal incident wave, or the integral of the reflection coefficient along some angle.

REVIEW OF PROFILE IMAGING

One of the most frequently used prestack depth migration techniques is the profile imaging scheme (Claerbout, 1985). The profile imaging concept says that reflectors exist in the earth at places where the downgoing wave is time-coincident with an upcoming wave. In profile migration methods, both the downgoing wave and the upcoming wave are extrapolated to a depth and followed by imaging.

The most straightforward imaging technique is to extract the zero lag of the cross-correlation of the two waves. The image is then created by displaying the zero-lagged cross-correlation everywhere in (x,z)-space. The image obtained by the cross-correlation imaging condition doesn't tell us much about the reflector itself because the amplitude of the zero-lagged cross-correlation depends not only on the reflection coefficient but also on the amplitude of the downgoing and upcoming wave at the reflector.

Let $U(\omega, x, z)$ and $D(\omega, x, z)$ be the upcoming and downgoing waves in the frequency domain, respectively. The zero lag of the cross-correlation can be represented by

$$Image(x, z) = \sum_{\omega} U(\omega, x, z) D^*(\omega, x, z) \tag{1}$$

where $*$ represents the complex conjugate. Since the upcoming wave can be approximated by the convolution of the downgoing wave with the reflectivity function, $R(x,z)$, Equation (1) can be rewritten as

$$Image(x,z) = R(x,z) \sum_{\omega} D(\omega,x,z) D^*(\omega,x,z) \tag{2}$$

The above equation tells us that the the image obtained by the zero lag cross-correlation represents the reflection coefficient scaled by the energy of the downgoing wave. The better reflection coefficient can be obtained from Equation (1) and (2) by

$$R(x,z) = \frac{\sum_{\omega} U(\omega,x,z) D^*(\omega,x,z)}{\sum_{\omega} D(\omega,x,z) D^*(\omega,x,z) + \epsilon^2} \tag{3}$$

In the above equation, ϵ^2 represents a small positive value that is introduces to stabilize because $D(\omega,x,z)$ may contain zeros.

The final image of the full prestack depth migration is usually obtained by summing all the shot profile images. Let's assume a spherical wavefront for each shot profile and a relatively gentle dip of the reflectors. Then the final image can be interpreted as the integral of the reflection coefficient over the incident angle because each shot has a different incident angle for the same reflection point. The real earth, however, does not involve such assumptions. The spherical wavefront is only valid in a constant velocity medium. Even in the constant medium, a reflector with complex shape does not allow regular samples in the incident angle for regularly spaced shots. Thus, the image of the conventional prestack migration only provide the reflector locations by mapping a value which is summation of many reflection coefficients shown from every shots.

This difficulty can be solved if we can control the incident angle at the reflector.

IMAGING BY WAVEFRONT SYNTHESIS

A "wave stack" is any stack over a common geophone gather in which the moveout is independent of time (Schultz and Claerbout, 1978). Huygens' principle permits the synthesis of arbitrarily shaped downward propagating wavefronts from the superposition of many spherical wavefronts. The migration of wave stacked data can be accomplished the same way as the profile imaging. Now the downgoing wave is the synthesized source array and the upcoming wave is the wave stacked data.

One of the most attractive features of the wave stack approach is computational efficiency. Stacking along common geophone gathers significantly reduces the size of the data space to be migrated. Compared to full prestack depth migration which requires the migration of each profile, the wave stack reduces the time for the migration process by two orders of magnitude.

Another advantage of the wave stack is the fact that it provides a way to get an image which represents the characteristics of the reflection coefficient in a consistent manner through all depth. The following two sections explain the features of the image obtained by various wavefront synthesis procedures.

Surface-oriented wavefront synthesis

Taner (1976) proposed to synthesize plane wave sources at the surface by stacking traces in a common receiver gather. The stacked section can be migrated with the same concept as profile imaging. Now the downgoing wave is a plane wave at the surface and the upcoming wave is the stacked traces. The image by this approach represents the reflection coefficient at the normal incidence angle for a horizontal reflector and a non-zero incidence angle for a dipping reflector if the velocity is constant.

Schultz and Claerbout (1978) note that reflectors of different dips can be shown more clearly and used to estimate the velocity by synthesizing various slanted plane waves. By using various slanted plane wave stacks, we can illuminate the dipping reflector with the maximum amplitude of the reflection coefficient.

This analysis, however, is valid only within the shallow depth levels because the incident plane or slanted wavefront will be distorted at deeper levels due to variations of the velocity. Thus we can have more interpretable images of reflectors only within the shallow regions.

Target-oriented wavefront synthesis

Rietveld et al. (1992) and Berkhout (1992) proposed a target-oriented wavefront synthesis for illuminating reflectors under a complex velocity overburden more clearly. Using the unitary property of the wavefield extrapolation operator, they generate a synthesis operator for a wave stack whose wavefront has a predefined shape at a certain subsurface location.

Suppose that we want to have a downgoing wavefield $D(\omega, x, z_n)$ at depth z_n. This wavefield can be obtained by propagating a certain wavefield at the surface, $D(\omega, x, z_0)$, to the depth level z_n.

$$D(\omega, x, z_n) = W(z_n, z_0) D(\omega, x, z_0) \tag{4}$$

where $W(z_n, z_0)$ represents a wave propagation operator from z_0 to z_n in forward time. If we know $D(\omega, x, z_n)$,then $D(\omega, x, z_0)$ can be found approximately using the unitary property of the propagation operator,

$$\tilde{D}(\omega, x, z_0) \sim W^*(z_0, z_n) D(\omega, x, z_n) \tag{5}$$

where $W^*(z_0, z_n)$ represents a wave propagation operator from z_n to z_0 in backward time. Equation (6) tells us that the areal shot (1992, Berkhout), $\tilde{D}(\omega, x, z_0)$ will approximately generate the predefined wavefield, $D(\omega, x, z_n)$, at depth z_n.

If we assume each shot gather, $U(w, x, z_0|x_s)$, is due to an impulse at x_s, the response of the areal shot can be synthesized by using the convolution formula as

$$\tilde{U}(\omega, x, z_0) = \sum_{x_s} \tilde{D}(\omega, x_s, z_0) U(w, x, z_0|x_s) \tag{6}$$

The imaging is performed in the same manner as profile imaging with $\tilde{U}(\omega, x, z_0)$ as the upcoming wave and $\tilde{D}(\omega, x, z_0)$ as the downgoing wave.

EXAMPLES

The various wave stack approaches, which were explained in the previous section, are tested using the well-known Marmousi dataset (Figure 1). Most of the wave stack approaches use a profile imaging method as the imaging tool. The profile imaging requires that every trace after wave stack have the information from all shots. This means that the ideal acquisition pattern should be a fixed spread acquisition (Figure 2). The Marmousi data set, however, used moving marine spread acquisition (Figure 3). This reality of the acquisition will result in some ghost images. One quick way to increase the coverage of the source for each trace in the stacked section is to use the reciprocity property. Figure 4 shows the coverage after applying reciprocity.

The result of the synthesis for a plane wave at the surface is shown in Figure 5. This synthesis is obtained by stacking along the common geophone gathers. Figure 6 shows the migrated image with the true velocity model (Figure 1). For extrapolation of both upcoming and downgoing wave, I used the split-step Fourier method (Stoffa at al., 1990). The images are generally located at the correct place, but show large amplitude variation along the same reflector. This effect are due to the distortion of the wavefront and the complex shape of the reflectors.

The result of the synthesis for a slanted plane wave at the surface is shown in Figure 8. For this synthesis, each shot was delayed from left to right with $p = .1(sec/km)$ and the delay operator is shown in Figure 7. In the Figure 9, which is the migrated image of Figure 8, shows the stronger amplitude along the dips that are approximately parallel to the wavefront.

Another slanted plane wave is synthesized with opposite direction at the surface. For this synthesis, the delay operator, $p = -.1(sec/km)$, are applied to each shot gathers and are shown in Figure 10. The result of wave stack is shown in Figure 11. Figure **??** shows the migrated image with the true velocity model (Figure 1).

For synthesizing a plane wave at 800 meters depth level, the synthesis operator is generated by equation (5) and shown in Figure 13. Figure 14 shows the wave stack by use of the synthesis operator Figure 13. Figure 15 shows the result of migration. Figure 17 shows the result of migration using the same procedures as the Figure 15 for a plane wave at depth level 2800 meter.

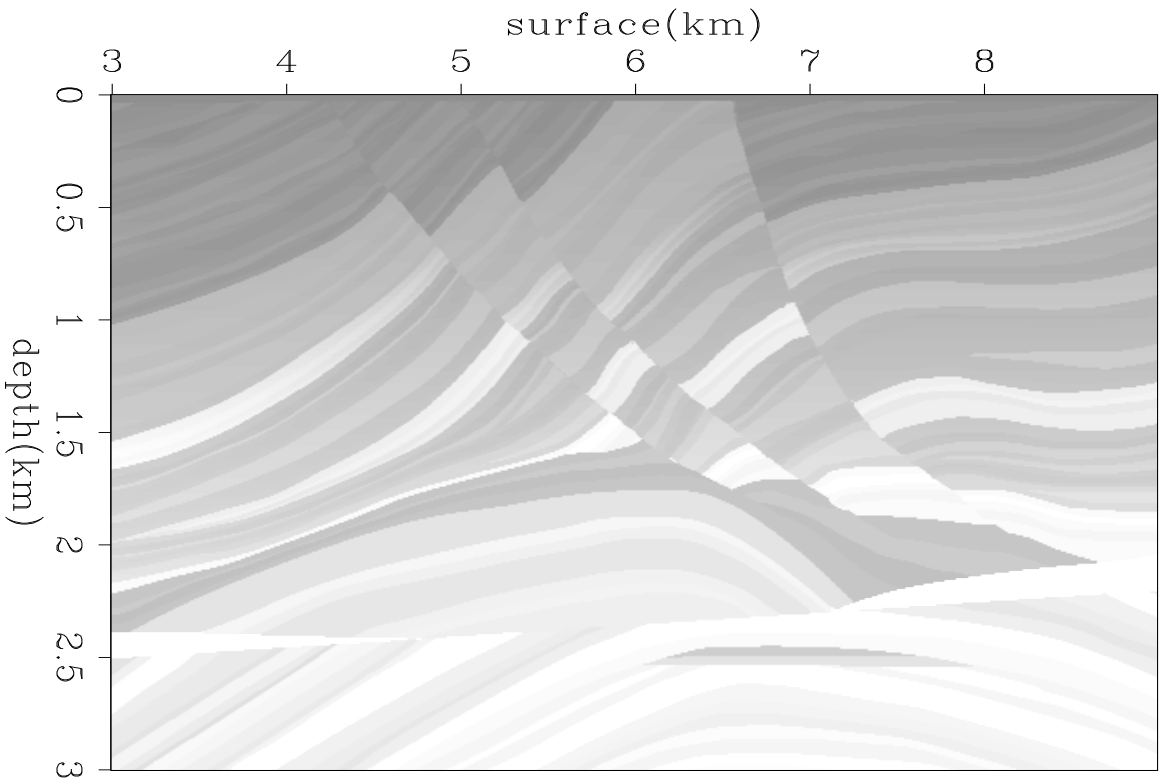

Figure 1: The Marmousi velocity model, cf. Versteeg and Grau(1991). jun-marmvelwin [NR]

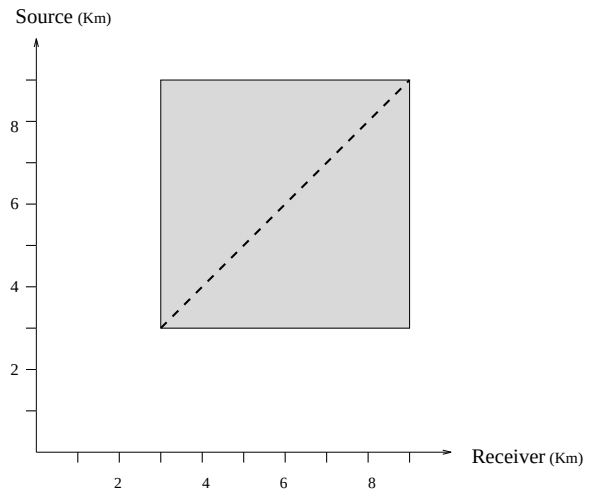

Figure 2: A fixed spread acquisition. The acquisition of this type is ideal for the controlled illumination because each trace after wave stack will have the responses from all shots. jun-idealgeom [NR]

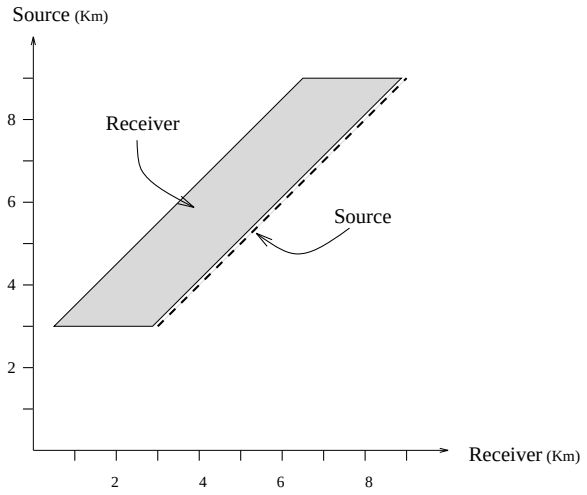

Figure 3: The marine spread acquisition of the Marmousi data set. jun-marmgeom [NR]

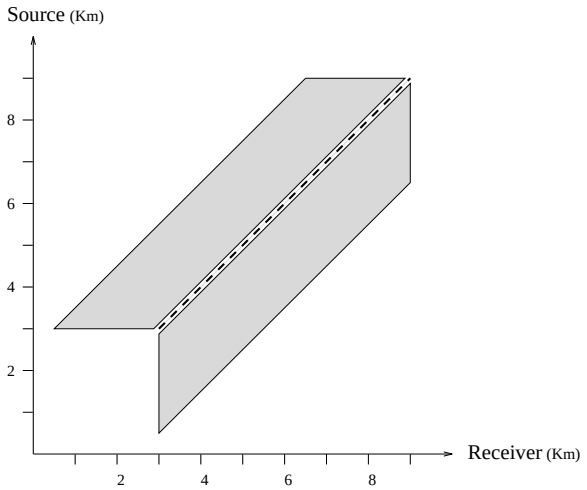

Figure 4: The Marmousi data set coverage after applying the reciprocity property of the source and receiver. jun-marmrecp [NR]

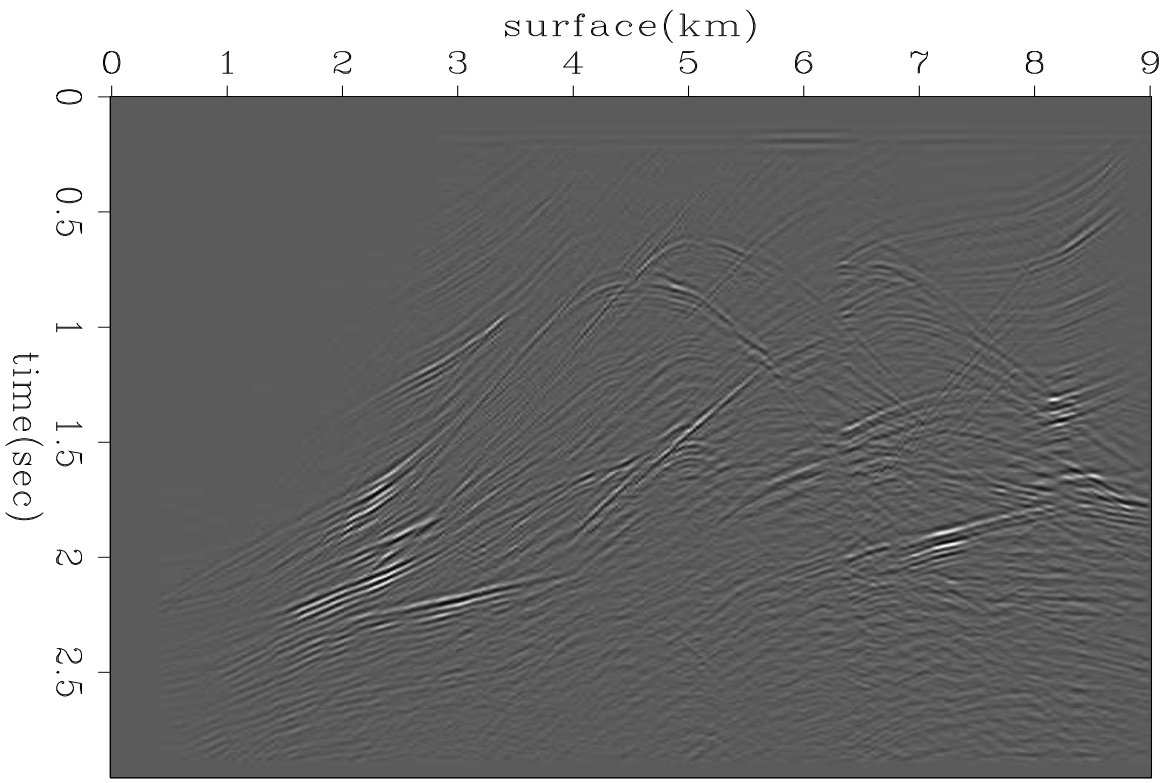

Figure 5: Stacked section by simulating a plane wave at the surface. jun-stackp1 [ER]

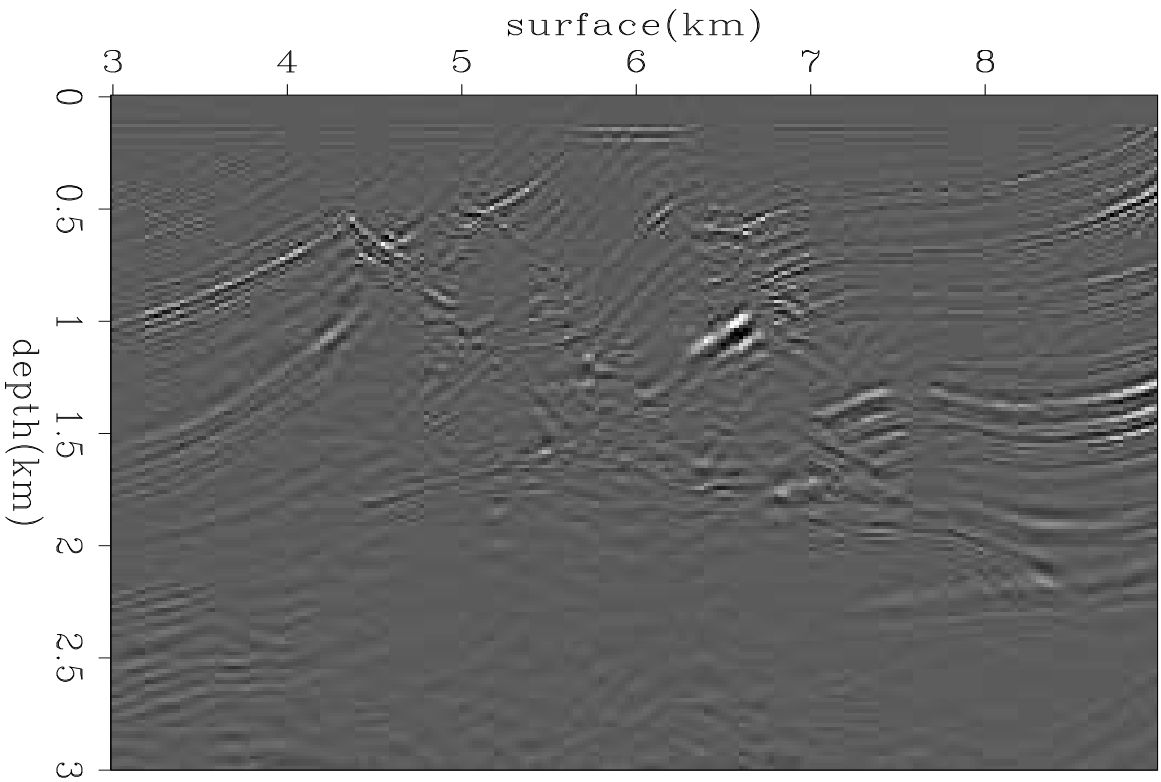

Figure 6: Migrated image of Figure 5. jun-conillp1 [ER]

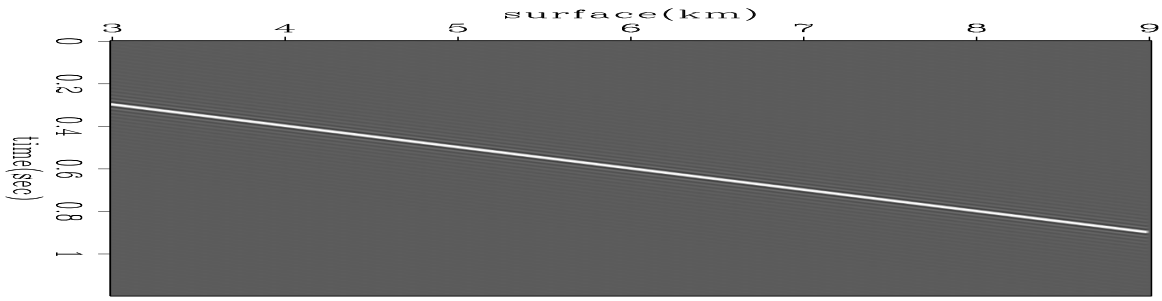

Figure 7: Synthesis operator for simulating slant plane wave: Each shot gather is delayed with $p = .1$ (sec/km) at the surface before wave stack along the common geophone gathers. jun-srcfldsp1-1 [ER]

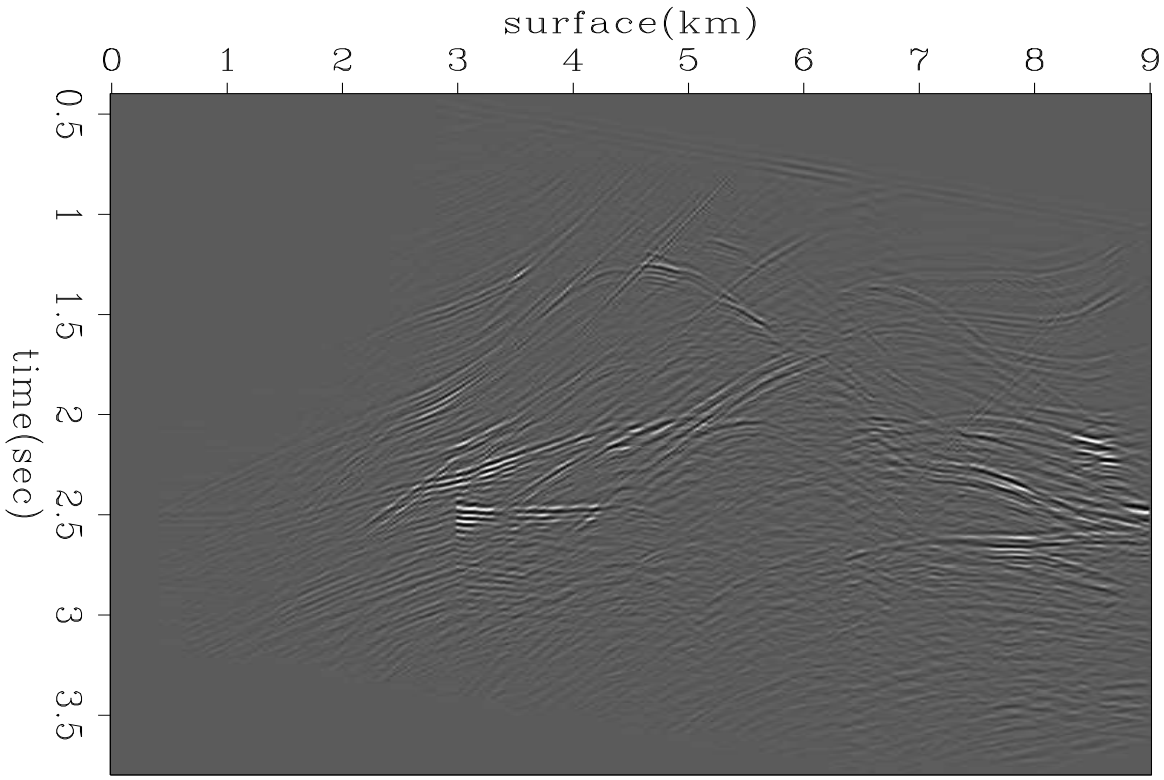

Figure 8: Stacked section by simulating a slanted plane wave (p=.1(sec/km)) at the surface. jun-stacksp1-1 [ER]

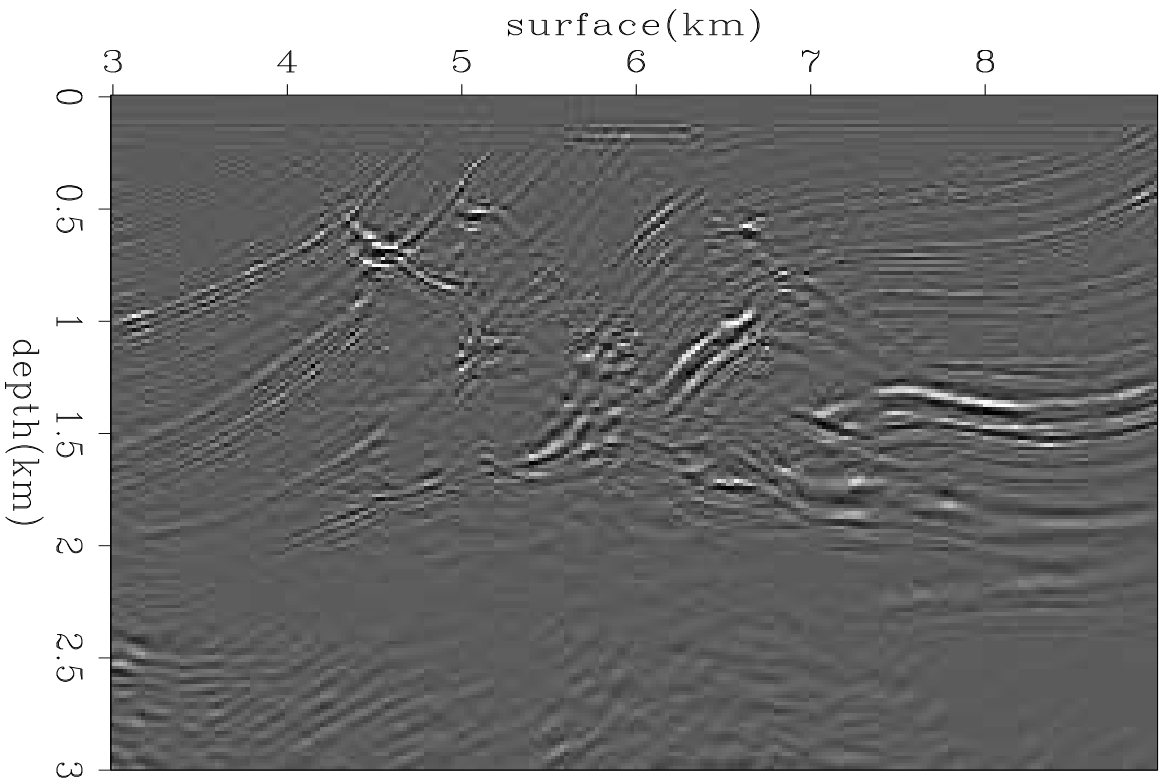

Figure 9: Migrated image of Figure 8. jun-conillsp1-1 [ER]

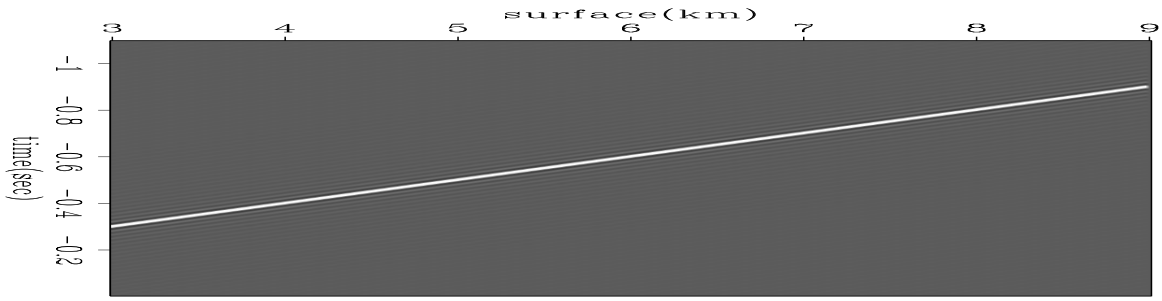

Figure 10: Synthesis operator for simulating slant plane wave: Each shot gather is delayed with $p = -.1$ (sec/km) at the surface before wave stack along the common geophone gathers. jun-srcfldns1-1 [ER]

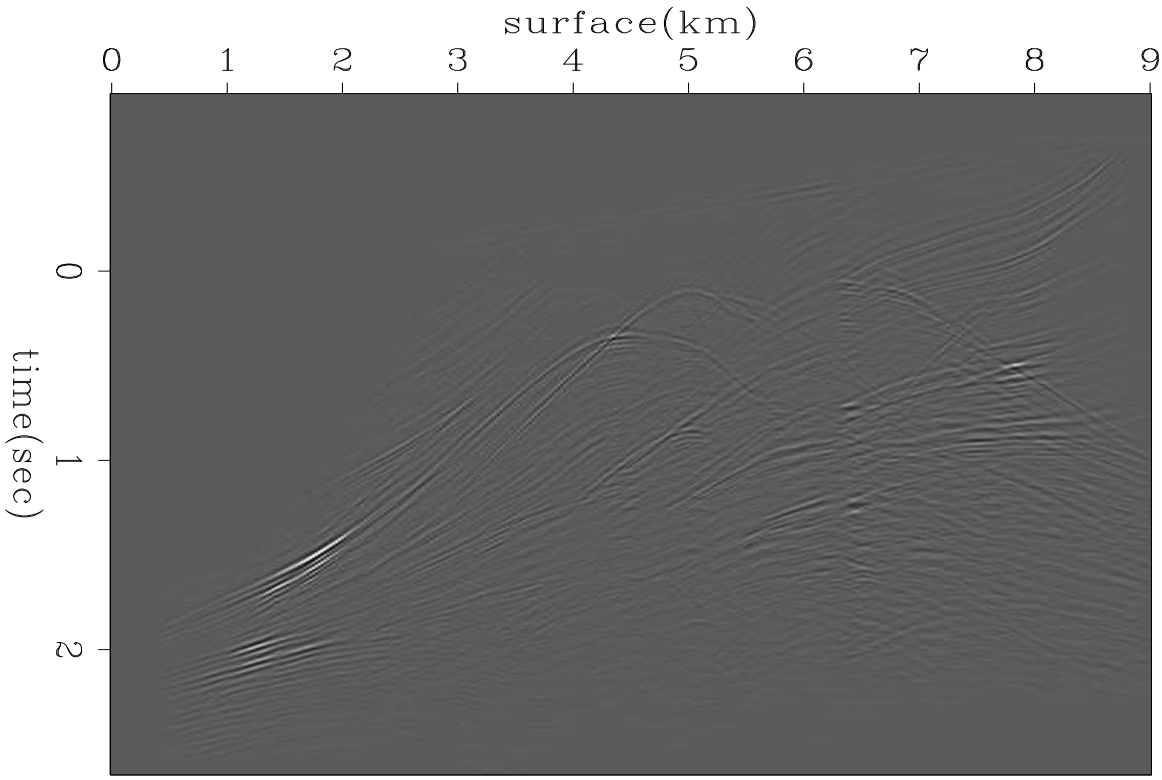

Figure 11: Stacked section by simulating a slanted plane wave (p=-.1(sec/km)) at the surface. jun-stackns1-1 [ER]

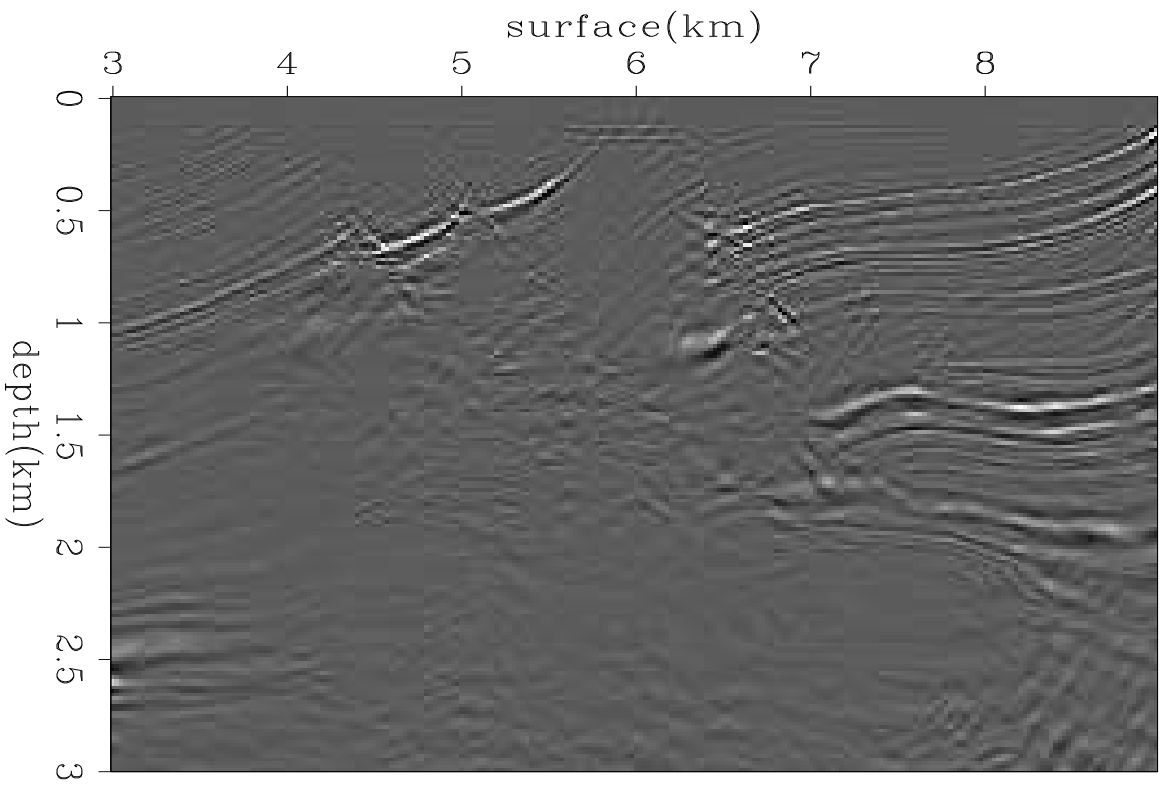

Figure 12: Migrated image of Figure 11. jun-conillns1-1 [ER]

We can see that the reflector at deep level start to appear as the level of plane wave synthesis goes down. Figure 18 is a result of summation of several images, plane wave synthesis at 0, 2000, 2800 meters and slanted plane wave synthesis at 800 meters.

DISCUSSIONS AND FUTURE PLANS

The testing of the controlled illumination method to Marmousi data shows very reasonable results. However, there are some aspects which can be improved.

One of the most important assumptions in this technique is the unitary property of the wave propagation operator. In the actual numerical implementation of the wave propagation operator, however, this assumption is not valid, especially when the velocity changes a lot. In such case, we should use inversion technique to find synthesis operator. One good candidate is least squares technique. Ji (1992) showed least square datuming can be done very fast using conjugate gradient method.

The other important factor is missing traces. Most of conventional acquisition patterns leaves many missing traces at near and far offset. For optimizing the controlled illumination process, interpolation of the near and far offsets is necessary. The

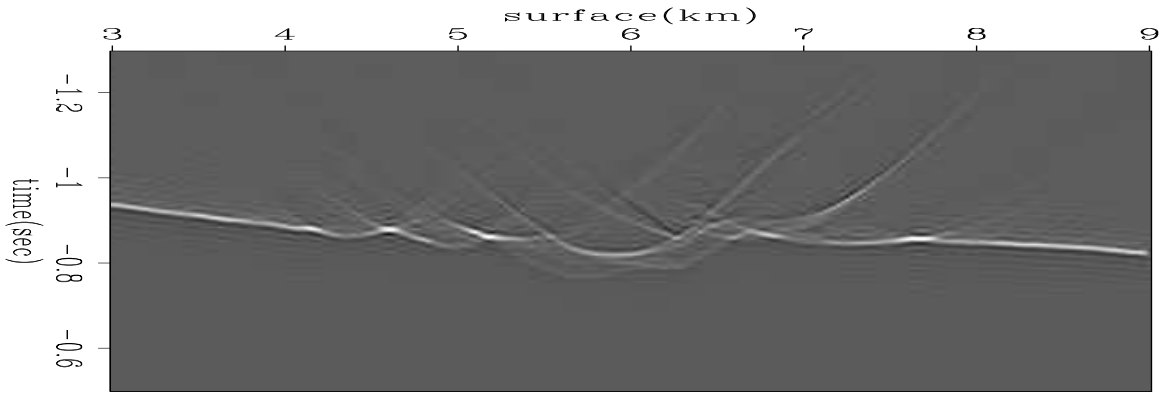

Figure 13: Synthesis operator for simulating plane wave at 800 meters. jun-srcfldp50 [ER]

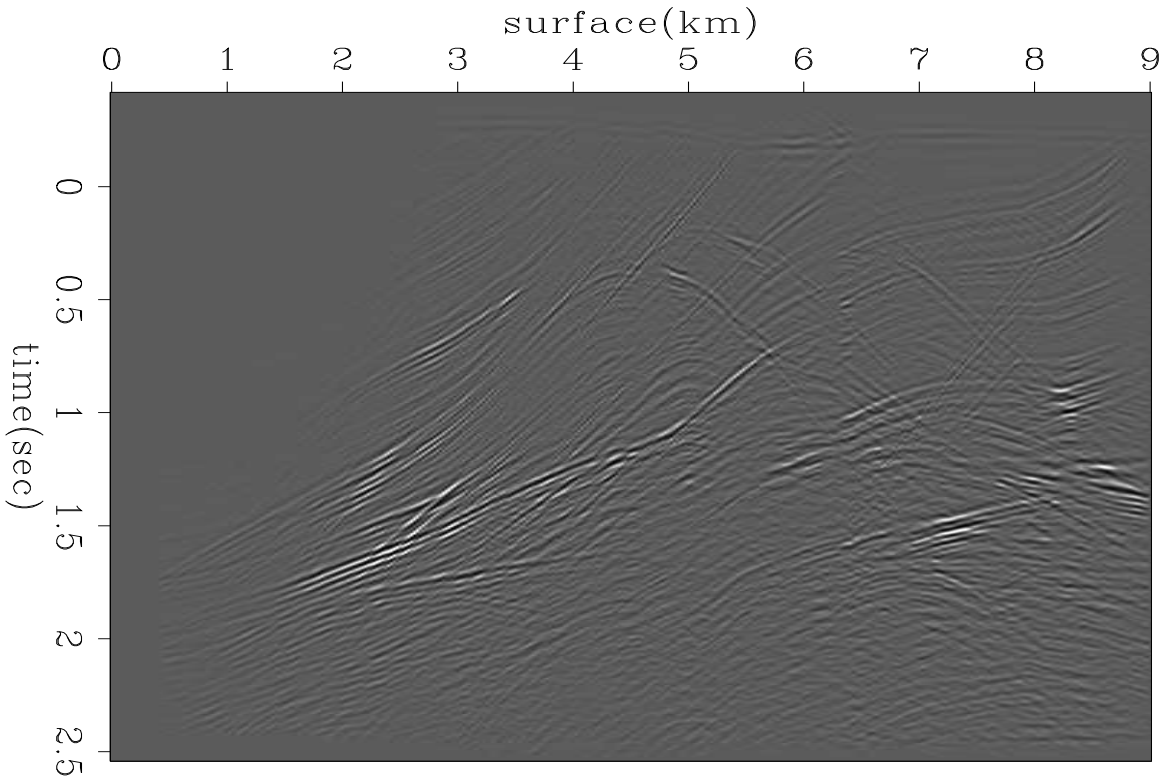

Figure 14: Wave stack section by simulating a plane wave at depth level 800 meter. jun-stackp50 [ER]

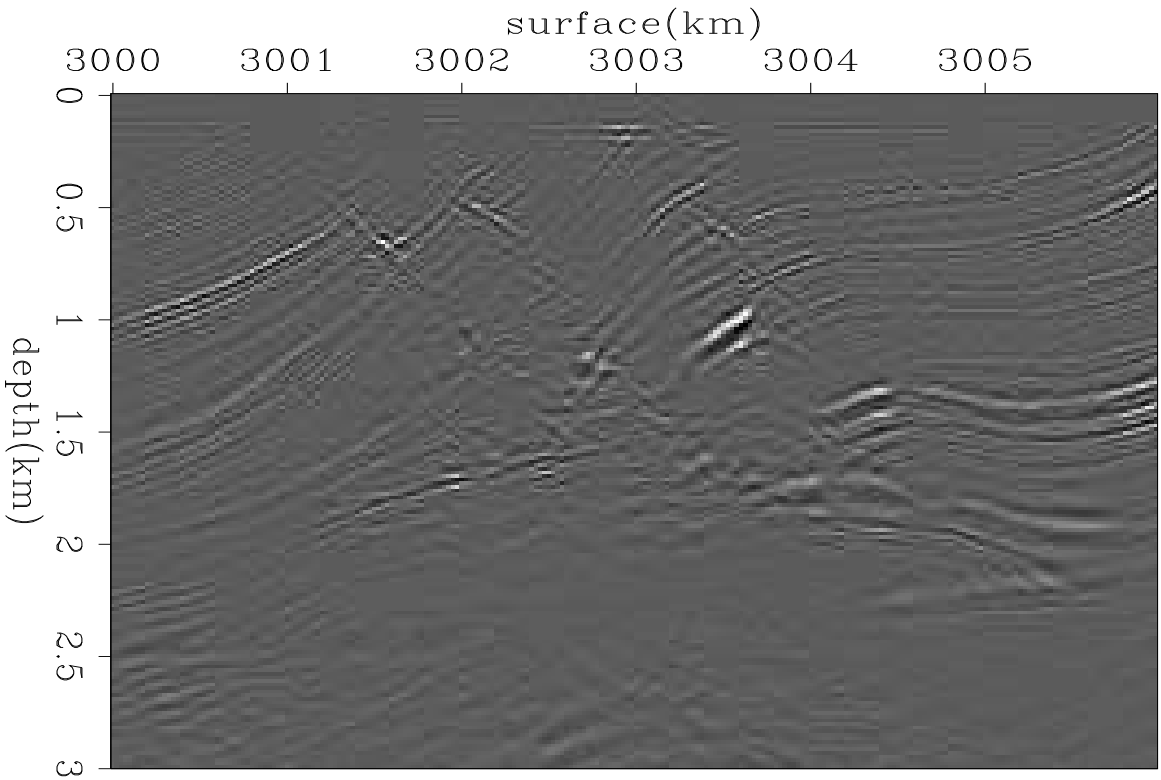

Figure 15: Migrated image of Figure 14. jun-conillp50 [ER]

interpolation scheme discussed by Ji and Claerbout (1991) in the CMP point domain would be a good candidate for this purpose. When we illuminate reflectors in a deep depth, the far offset information is very important.

In the future, I'll apply the least-squares technique to find the synthesis operator and consider many interpolation algorithms to improve the resolution of the deep reflector images.

REFERENCES

Berkhout, A. J., 1992, Areal shot record technology: Journal of Seismic Exploration, **1**, 251–264.

Claerbout, J. F., 1985, Imaging the Earth's Interior: Blackwell Scientific Publications.

Ji, J., 1992, Least squares imaging, datuming, and interpolation using the wave equation: SEP–**75**, 141–160

Ji, J and Claerbout, J. F., 1991, Trace interpolation using a recursive dip filter: SEP–**72**, 43–55

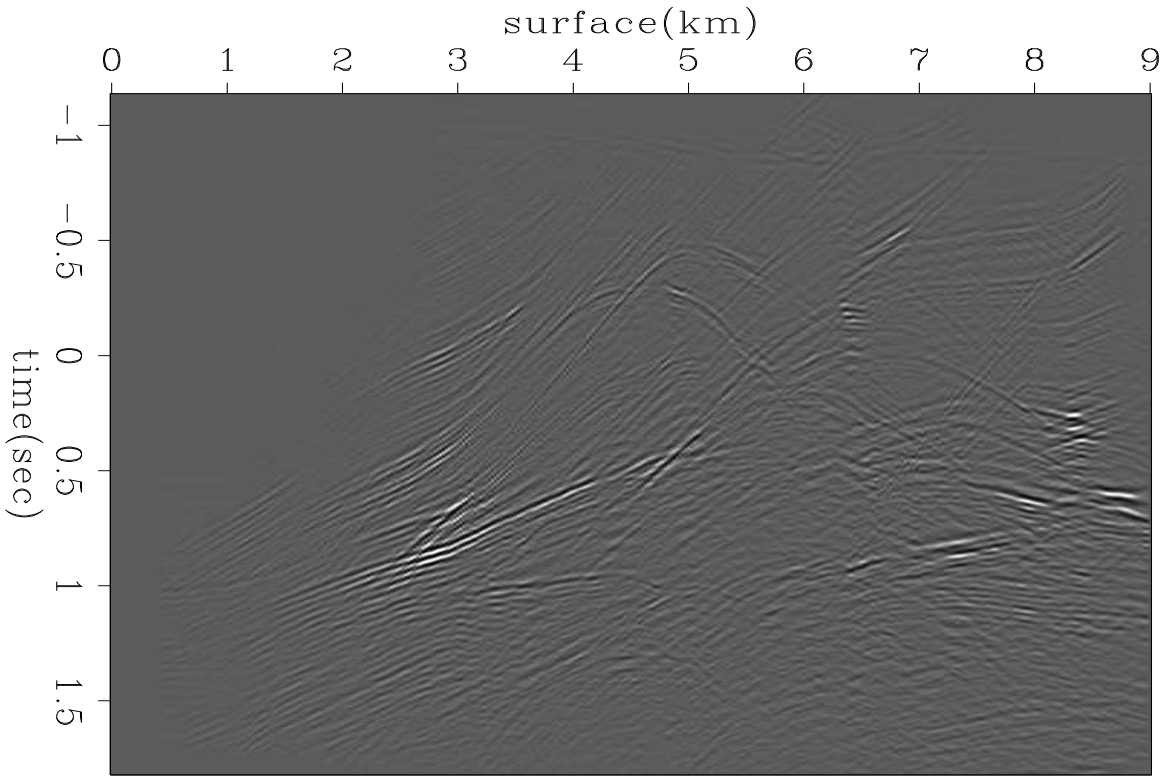

Figure 16: Wave stack section by simulating a plane wave at depth level 2800 meter. jun-stackp175 [ER]

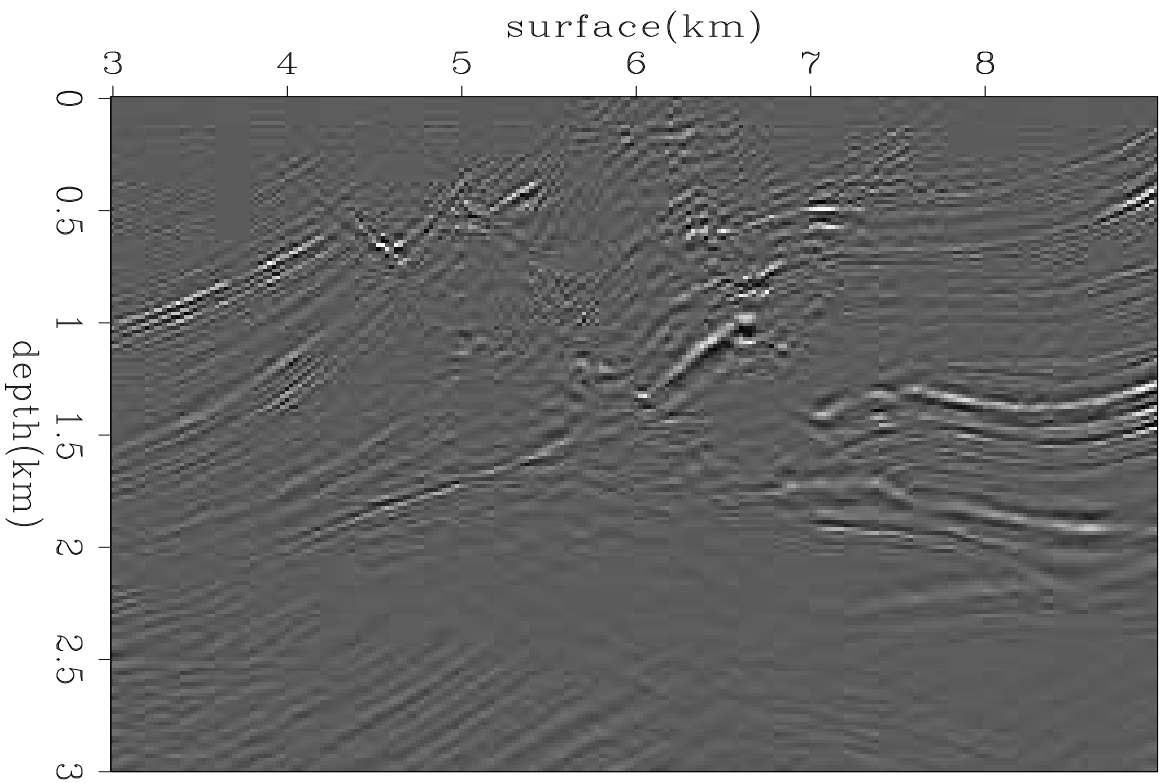

Figure 17: Migrated image of Figure 16. jun-conillp175 [ER]

Rietveld, W. E. A., Berkhout, A. J., and Wapenaar, C. P. A., 1992, Optimum seismic illumination of hydrocarbon reservoirs: Geophysics, **57**, 1334–1345.

Rietveld, W. E. A. and Berkhout, A. J., 1992, Depth migration combined with controlled illumination: 62th Ann. Internat. Mtg., Soc. Expl. Geophys., Expanded Abstracts, 931–934.

Schultz, P. S., 1978, Velocity estimation and downward continuation by wavefront synthesis: Geophysics, **43**, 691–714.

Stoffa, P. L., Fokkema, J. T., de Luna Freire, R. M., and Kessinger, W. P., 1990, Split-step Fourier migration: Geophysics, **55**, 410–421.

Taner, M. T., 1976, Simplan: simulated plane-wave exploration: 46th Ann. Internat. Mtg., Soc. Expl. Geophys., Expanded Abstracts, 186–187.

Versteeg, R and Grau, G. 1991, The Marmousi experience: proceedings of the 1990 EAEG workshop on practical aspects of seismic data inversion, EAEG.

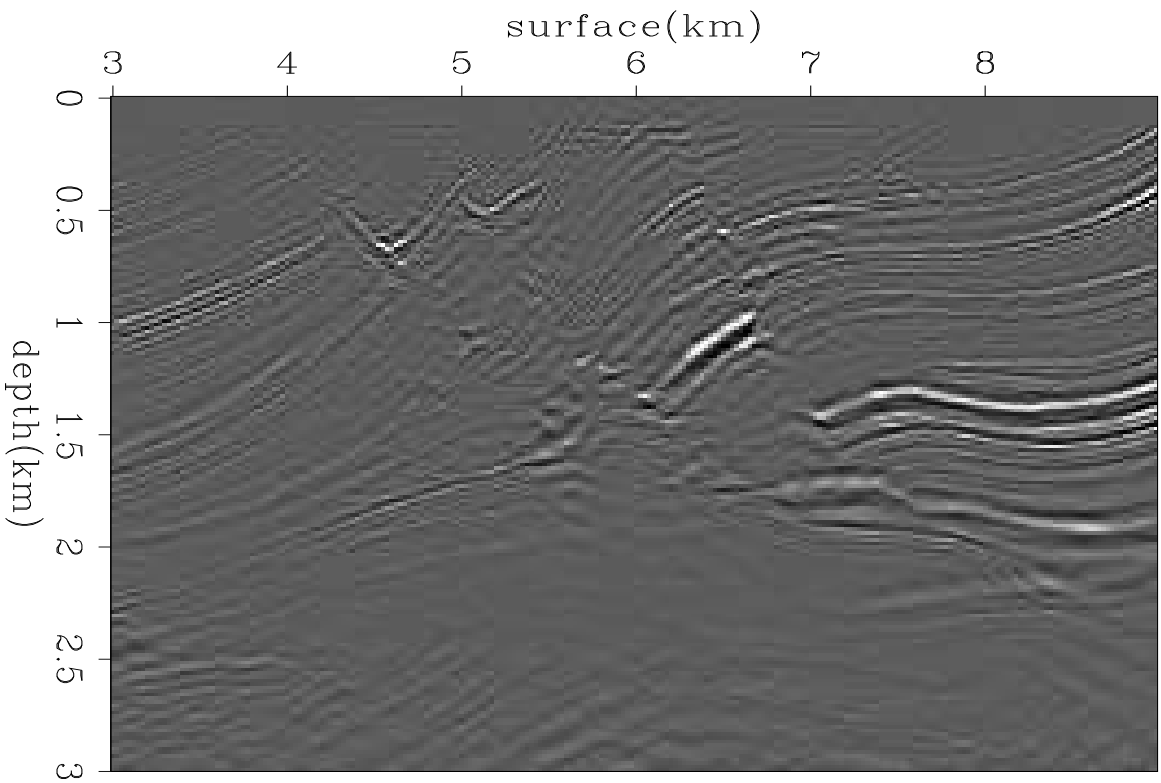

Figure 18: Migrated image using controlled illumination by simulating several plane waves at different depth levels: plane waves at 0, 2000, and 2800 meters, and two slanted plane waves at 800 meters. jun-conillpsum [ER]